Physics of Fluids ARTICLE pubs.aip.org/aip/pof

A Josephson–Anderson relation for drag in classical channel flows with streamwise periodicity: Effects of wall roughness

Cite as: Phys. Fluids **36**, 093113 (2024); doi: 10.1063/5.0226226
Submitted: 30 June 2024 · Accepted: 27 August 2024 ·
Published Online: 16 September 2024

Samvit Kumar[a)] and Gregory L. Eyink[a)]

AFFILIATIONS

Department of Applied Mathematics and Statistics, The Johns Hopkins University, Baltimore, Maryland 21218, USA

Note: This paper is part of the special topic, K. R. Sreenivasan: A Tribute on the occasion of his 75th Birthday.
[a)]**Authors to whom correspondence should be addressed:** skumar67@jh.edu and eyink@jhu.edu

ABSTRACT

The detailed Josephson–Anderson relation equates the instantaneous work by pressure drop over any streamwise segment of a general channel and the wall-normal flux of spanwise vorticity spatially integrated over that section. This relation was first derived by Huggins for quantum superfluids, but it holds also for internal flows of classical fluids and for external flows around solid bodies, corresponding there to relations of Burgers, Lighthill, Kambe, Howe, and others. All of these prior results employ a background potential Euler flow with the same inflow/outflow as the physical flow, just as in Kelvin's minimum energy theorem, so that the reference potential incorporates information about flow geometry. We here generalize the detailed Josephson–Anderson relation to streamwise periodic channels appropriate for numerical simulation of classical fluid turbulence. We show that the original Neumann b.c. used by Huggins for the background potential creates an unphysical vortex sheet in a periodic channel, so that we substitute instead Dirichlet b.c. We show that the minimum energy theorem still holds and our new Josephson–Anderson relation again equates work by pressure drop instantaneously to integrated flux of spanwise vorticity. The result holds for both Newtonian and non-Newtonian fluids and for general curvilinear walls. We illustrate our new formula with numerical results in a periodic channel flow with a single smooth bump, which reveals how vortex separation from the roughness element creates drag at each time instant. Drag and dissipation are thus related to vorticity structure and dynamics locally in space and time, with important applications to drag-reduction and to explanation of anomalous dissipation at high Reynolds numbers.

I. INTRODUCTION

The modern paradigm[1,2] for drag and dissipation in the theory of quantum superfluids arose from the work of Josephson[3] for superconductors and of Anderson[4] for neutral superfluids, who both noted a time-average relation between drops of voltage/pressure in flow through wires/channels and the cross-stream flux of quantized magnetic-flux/vortex lines. It was subsequently shown by Huggins[5] that a "detailed Josephson–Anderson (JA) relation" holds between instantaneous work by pressure drop and integrated flux of vorticity across the mass flux of the background potential associated with the ground-state quantum superflow. These results are the basis of contemporary solutions to the "drag reduction" problem in high-temperature superconductors, where, above some critical current, nucleation and motion of magnetic vortices create an effective voltage drop and loss of superconductivity. The remedy is to introduce impurities and disorder to pin the vortices and prevent their cross-stream motion, thus restoring dissipationless flow of electric current.[6,7]

It was noted by Anderson[4] and by Huggins[5] that corresponding results hold for classical fluids described by the viscous Navier–Stokes equations. Eyink[8] pointed out that the time-average result had been invoked already by Taylor[9] for classical turbulent pipe flow and that an instantaneous relation between pressure gradients and vorticity flux at solid surfaces was derived by Lighthill,[10] both anticipating the results for quantum fluids. Subsequently, Eyink[11] showed that Huggins's detailed Josephson–Anderson relation holds also for external flows around solid bodies, relating drag on the body instantaneously to the integrated flux of vorticity across the streamlines of the background potential flow. As reviewed by Biesheuvel and Hagmeijer,[12] closely related instantaneous relations for drag in external flows of classical fluids had been previously derived by Burgers, Lighthill and others, especially Howe,[13] and applied to both laminar and turbulent flow regimes. However, to our knowledge there has been no prior study applying the detailed relation of Huggins[5] to classical channel flows, either laminar or turbulent. Previous work of Huggins,[14] Eyink,[8] and Kumar *et al.*[15] has investigated classical turbulent channel flow using only the time-averaged relation of Taylor[9] and Anderson,[4] rather than the detailed relation which reveals the instantaneous connection between drag and vorticity dynamics.

We shall show in this paper that the detailed Josephson–Anderson relation in the original form of Huggins[5] has, in fact, a significant flaw when applied to classical fluid turbulence. The origin of the problem is Huggins's assumption that the channel inflow and outflow are pure potential, which is realistic for many superfluid applications where the quantum vortex tangle is strictly confined to some interior section of the channel. However, in applications to classical fluid turbulence this assumption is quite unrealistic as the outflow and very commonly the inflow as well consist of highly rotational flow. Furthermore, we shall see that Huggins's original derivation, when carried out with the streamwise periodic boundary conditions that are most common in numerical simulations, introduces a spurious vortex sheet into the reference "potential" flow. To avoid these serious difficulties, we show here that it suffices to use instead a reference potential, which matches only the mean mass flux of the physical flow and not the instantaneous inflow and outflow fields. We show, nevertheless, that the original derivation of Huggins[5] goes through with only minor modifications for this new choice of potential and yields again an instantaneous relation between work by pressure drop and spatially integrated vorticity flux. We then present a sample numerical application for periodic channel flow with a single smooth bump at modest Reynolds number, but sufficiently high that flow separation is observed with shedding of a rotational wake. In this flow, we relate the instantaneous drag arising from both skin friction and pressure forces (form drag) to the vorticity flux from the boundary arising from separation. Our results thus reveal a deep unity to the origin of drag in both classical and quantum fluids.

The results presented here build upon the pioneering work of K. R. Sreenivasan, who has made seminal contributions to turbulence in both quantum and classical fluids. In particular, Bewley *et al.*[16] and Fonda, Sreenivasan, and Lathrop[17,18] developed the first experimental methods to visualize quantized vortices in a superfluid flow and to verify the reconnection dynamics, which has been widely theorized to account for superfluid turbulent dissipation, going back to Feynman.[19] We shall discuss below the relation of our results with such reconnection processes. In addition, Sreenivasan[20] and Sreenivasan and Sahay[21] have made fundamental contributions to the Reynolds-number scaling of turbulent wall-bounded flows, continuing in more recent works.[22,23] The persistent viscous effects identified by Sreenivasan and Sahay[21] make a very important contribution, in particular, to vorticity flux[8,15] in wall-bounded flows, which is very relevant to our subject. Finally, the detailed Josephson–Anderson relation has direct applications to problems of polymer drag reduction studied by Sreenivasan and White[24] and turbulent energy dissipation rate studied in classic works of Sreenivasan,[25,26] and Meneveau and Sreenivasan[27] which we discuss briefly below. A great legacy of Sreeni's research career is a strong interdisciplinary point of view and a search for general unifying principles, an example which we strive to emulate in this contribution to the Special Issue in honor of his 75th birthday.

II. PRIOR WORK OF HUGGINS AND OTHERS

In this section, we very briefly review the detailed relation of Huggins, its derivation, and the closely related results obtained by others for external flows. Huggins[5] considered a classical incompressible fluid at constant mass density ρ and with kinematic viscosity ν subject to accelerations both from a conservative force $-\nabla Q$ and from a non-conservative force $-\mathbf{f}$ satisfying $\boldsymbol{\nabla}\times\mathbf{f}\neq\mathbf{0}$, described by the incompressible Navier–Stokes equation written as

$$\partial_t \mathbf{u} = \mathbf{u}\times\boldsymbol{\omega} - \nu\boldsymbol{\nabla}\times\boldsymbol{\omega} - \boldsymbol{\nabla}(p + |\mathbf{u}|^2/2 + Q) - \mathbf{f}. \tag{1}$$

A fundamental step made by Huggins[14,28] was to rewrite the above momentum balance in the form

$$\partial_t u_i = (1/2)\varepsilon_{ijk}\Sigma_{jk} - \partial_i h, \tag{2}$$

with anti-symmetric *vorticity flux tensor*

$$\Sigma_{ij} = u_i\omega_j - u_j\omega_i - \nu(\partial_i\omega_j - \partial_j\omega_i) - \varepsilon_{ijk}f_k, \tag{3}$$

and *total pressure*

$$h = p + |\mathbf{u}|^2/2 + Q, \tag{4}$$

including both the hydrostatic and the dynamic pressures. The tensor Σ_{ij} represents the flux of the jth vorticity component in the ith coordinate direction, with the first term on the RHS in (3) describing advection, the second stretching/tilting/twisting, the third viscous diffusion, and the fourth the Magnus effect of the body force. This interpretation of the tensor is made clear by taking the curl of the momentum equation (1), which yields a local conservation law for vector vorticity

$$\partial_t\omega_j + \partial_i\Sigma_{ij} = 0. \tag{5}$$

Equation (2) thus shows directly the connection between momentum balance and vorticity transport, and this equation is itself the most elementary version of the classical Josephson–Anderson relation.

To derive his detailed relation, Huggins[5] considered very general flows through pipes and channels, whose walls might be curved or bent, with rough or wavy surfaces, and with variable cross sections. For example, a flow through an orifice in a wall is a classical application of the JA-relation in superfluids. See Fig. 1 for the general situation. Huggins assumed given velocity at the inflow surface S_{in} and at the outflow surface S_{out} and stick boundary conditions at the sidewall S_w

$$\mathbf{u}|_{S_{in}} = \mathbf{u}_{in}, \quad \mathbf{u}|_{S_{out}} = \mathbf{u}_{out}, \quad \mathbf{u}|_{S_w} = \mathbf{0}. \tag{6}$$

A key idea of Huggins[5] was to compare the viscous rotational flow solving the incompressible Navier–Stokes equation (1) with an ideal incompressible potential flow $\mathbf{u}_\phi = \boldsymbol{\nabla}\phi_N$ solving the Euler equations with the same in-flow and out-flow,

$$\mathbf{n}\cdot\mathbf{u}_\phi|_{S_{in}} = \mathbf{n}\cdot\mathbf{u}_{in}, \quad \mathbf{n}\cdot\mathbf{u}_\phi|_{S_{out}} = \mathbf{n}\cdot\mathbf{u}_{out}, \quad \mathbf{n}\cdot\mathbf{u}_\phi|_{S_w} = 0, \tag{7}$$

where $\mathbf{n}$ is the unit normal at the boundary pointing into the fluid interior. In superfluid applications, this potential flow corresponds to the dissipation-less flow in the quantum ground state in the absence of any quantized vortex excitations. This is, in fact, the flow with the least energy among all incompressible flows with the boundary conditions

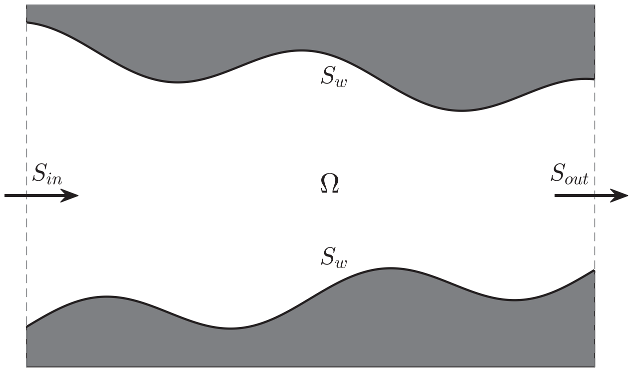

FIG. 1. Context of the detailed relation of Huggins:[5] Flow through a channel Ω with inflow surface S_{in}, outflow surface S_{out}, and sidewalls S_w.

(7) according to the Kelvin minimum energy theorem;[29–32] see also below. The scalar potential ϕ_N solves the Laplace equation $\nabla^2\phi_N = 0$ in the open flow domain Ω with Neumann boundary conditions supplied by (7) and is thus unique up to a spatial constant. In that case, the Euler dynamics reduce to the Bernoulli equation,

$$\partial_t\phi_N + \frac{1}{2}|\mathbf{u}_\phi|^2 + p_\phi + Q = c(t), \tag{8}$$

for a spatial constant $c(t)$, which yields the static Euler pressure p_ϕ and the total Euler pressure $h_\phi = p_\phi + |\mathbf{u}_\phi|^2/2 + Q$ given the velocity potential ϕ_N. It is a direct consequence of (8) that the potential Euler solution experiences no mean drag, since long-time averaging denoted by $\langle\cdot\rangle$ yields the relation

$$\langle\nabla h_\phi\rangle = \mathbf{0}, \tag{9}$$

and thus mass flux occurs without any mean gradient of the total pressure. Likewise, in terms of the kinetic energy of the potential flow,

$$E_\phi = (\rho/2)\int_\Omega |\mathbf{u}_\phi|^2 dV, \tag{10}$$

one finds using the Bernoulli equation (8) that

$$\begin{aligned}\frac{dE_\phi}{dt} &= \rho\int_\Omega \mathbf{u}_\phi\cdot\nabla(\partial_t\phi_N)\,dV = -\rho\int_{\partial\Omega}(\partial_t\phi_N)\mathbf{u}_\phi\cdot\mathbf{n}\,dA\\ &= \int_{S_{in}} h_\phi\,dJ - \int_{S_{out}} h_\phi\,dJ := \mathscr{W}_\phi,\end{aligned} \tag{11}$$

where $dJ = \rho\mathbf{u}_\phi\cdot d\mathbf{A}$ is the mass flux element along the potential flow and where the last line defines the instantaneous rate of work $\mathscr{W}_\phi$ done by the potential pressure h_ϕ. As long as the inflow/outflow conditions remain bounded in time, then also E_ϕ remains bounded and long-time averaging yields

$$\langle\mathscr{W}_\phi\rangle = 0. \tag{12}$$

The relations (9) and (12) may be regarded as analogues of the "d'Alembert paradox"[33,34] for potential fluid flows through pipes and channels.

The detailed relation of Huggins[5] connected vortex motion further to energy balance. It was natural in Huggins's analysis to adopt as reference the potential flow $\mathbf{u}_\phi = \nabla\phi_N$, which represents the superfluid velocity in the quantum ground state. Huggins thus decomposed the rate of work by the total pressure head,

$$\mathscr{W} = \int_{S_{in}} h\,dJ - \int_{S_{out}} h\,dJ, \tag{13}$$

as $\mathscr{W} = \mathscr{W}_\phi + \mathscr{W}_\omega$, where

$$\mathscr{W}_\omega = \int_{S_{in}} h_\omega\,dJ - \int_{S_{out}} h_\omega\,dJ \tag{14}$$

is the rate of work done by the head of *total rotational pressure* $h_\omega = h - h_\phi$. Because of (12), $\mathscr{W}_\omega$ represents the "effective work," which solely contributes to the long-time average. The main result of Huggins states that $\mathscr{W}_\omega$ is exactly equal to another quantity $\mathscr{T}$ that measures the flux of vorticity across the mass current of the background potential, given by the following equivalent expressions:

$$\begin{aligned}\mathscr{T} &= -\int_\Omega \rho\mathbf{u}_\phi\cdot(\mathbf{u}\times\boldsymbol{\omega} - \nu\nabla\times\boldsymbol{\omega} - \mathbf{f})\,dV\\ &= -\int dJ\int(\mathbf{u}\times\boldsymbol{\omega} - \nu\nabla\times\boldsymbol{\omega} - \mathbf{f})\cdot d\boldsymbol{\ell}\\ &= -\frac{1}{2}\int dJ\int \varepsilon_{ijk}\Sigma_{ij}d\ell_k,\end{aligned} \tag{15}$$

where the line integrals are along streamlines of the potential flow. In fact, we shall see that $\mathscr{T}$ represents a transfer of kinetic energy from potential to rotational motions. The *detailed Josephson–Anderson relation* of Huggins[5] then states precisely the identity

$$\mathscr{W}_\omega = \mathscr{T}. \tag{16}$$

In other words, the effective rate of work done by the rotational pressure head is instantaneously related to the transverse motion of vortex lines across the potential flow. This relation is useful precisely because $\mathscr{W}_\omega$ is the work contribution which is hard to understand and to compute, whereas $\mathscr{W}_\phi$ has transparent meaning and ϕ is computable at each time instant by standard solvers for the Laplace equation.

Because we must generalize this result for classical turbulent channel flow, it is useful to reprise here the short proof. Huggins[5] obtained (16) by deriving a complementary equation for the rotational fluid motions and by then considering the coupled energy balances for potential and rotational flows. The rotational velocity field defined by Huggins was $\mathbf{u}_\omega := \mathbf{u} - \mathbf{u}_\phi$, which accounts for all vorticity in the flow. Its governing equations are easily obtained by subtracting the Euler equation for $\mathbf{u}_\phi$ from the Navier–Stokes (1), yielding

$$\partial_t\mathbf{u}_\omega = \mathbf{u}\times\boldsymbol{\omega} - \nu\nabla\times\boldsymbol{\omega} - \nabla h_\omega, \tag{17}$$

where h_ω can be rewritten (up to a spatial constant) as

$$h_\omega = h + \partial_t\phi_N = p_\omega/\rho + |\mathbf{u}_\omega|^2/2 + \mathbf{u}_\omega\cdot\mathbf{u}_\phi, \tag{18}$$

with $p_\omega = p - p_\phi$ and $\mathbf{u}_\omega$ satisfies the boundary conditions

$$\begin{gathered}\mathbf{u}_\omega|_{S_{in}} = (\mathbf{u}-\mathbf{u}_\phi)|_{S_{in}}, \quad \mathbf{u}_\omega|_{S_{out}} = (\mathbf{u}-\mathbf{u}_\phi)|_{S_{out}},\\ \mathbf{u}_\omega|_{S_w} = -\mathbf{u}_\phi|_{S_w}.\end{gathered} \tag{19}$$

In particular,

$$\mathbf{n}\cdot\mathbf{u}_\omega|_{S_{in}} = \mathbf{n}\cdot\mathbf{u}_\omega|_{S_{out}} = \mathbf{n}\cdot\mathbf{u}_\omega|_{S_w} = 0. \tag{20}$$

The latter render the potential velocity $\mathbf{u}_\phi$ and the rotational velocity $\mathbf{u}_\omega$ orthogonal, since their spatial L^2 inner product is

$$\int_\Omega \mathbf{u}_\phi \cdot \mathbf{u}_\omega dV = \int_\Omega \nabla \cdot (\phi_N \mathbf{u}_\omega) dV = -\int_{\partial\Omega} \phi_N \mathbf{u}_\omega \cdot \mathbf{n}\, dS = 0. \quad (21)$$

This orthogonality is the essence of Kelvin's minimum energy theorem, since it implies that the total kinetic energy $E = (\rho/2)\int_\Omega |\mathbf{u}|^2 dV$ in the channel is a sum of potential and rotational contributions, $E = E_\phi + E_\omega$, with the kinetic energy of rotational motions given by

$$E_\omega = (\rho/2)\int_\Omega |\mathbf{u}_\omega|^2 dV.$$

In that case, the minimum kinetic energy E for all incompressible velocity fields $\mathbf{u}$ satisfying the b.c. (7) is obviously achieved with $\mathbf{u}_\omega = \mathbf{0}$ or $\mathbf{u} = \mathbf{u}_\phi$.

From the above equations, Huggins[5] derived balance equations for E_ω and E_ϕ. Taking the dot product of (17) with $\rho\mathbf{u}_\omega$ and integrating over the channel volume yields

$$\frac{dE_\omega}{dt} = \mathscr{T} - \mathscr{D} + \int_{S_{in}} h_\omega \mathbf{u}_\omega \cdot \mathbf{n}\, dA + \int_{S_{out}} h_\omega \mathbf{u}_\omega \cdot \mathbf{n}\, dA, \quad (22)$$

so that the b.c. (20) give the final equation for E_ω as

$$\frac{dE_\omega}{dt} = \mathscr{T} - \mathscr{D}, \quad (23)$$

where $\mathscr{T}$ is given by (15) and the total energy dissipation by non-conservative forces is given by

$$\mathscr{D} = \int_\Omega (\eta|\boldsymbol{\omega}|^2 + \rho\mathbf{u}\cdot\mathbf{f})\, dV,$$

with $\eta = \nu\rho$ the shear viscosity. The total energy satisfies of course the standard balance

$$\frac{dE}{dt} = \mathscr{W} - \mathscr{D}. \quad (24)$$

The equation for E_ϕ is then obtained simply by subtracting Eqs. (24) and (23), yielding

$$\frac{dE_\phi}{dt} = \mathscr{W} - \mathscr{T}. \quad (25)$$

The two balance equations (23) and (25) show that the work $\mathscr{W}$ done by the pressure head goes entirely into potential flow energy, which is, in turn, transferred by vortex motion through the term $\mathscr{T}$ into rotational flow energy, and then ultimately disposed by the dissipation $\mathscr{D}$ due to viscosity and other non-ideal forces acting on the rotational flow. As a final step, Huggins[5] then substituted the relation (11) for dE_ϕ/dt into (25) which, recalling the definition $\mathscr{W}_\omega := \mathscr{W} - \mathscr{W}_\phi$, yields directly the detailed Josephson–Anderson relation (16).

The previous results are very closely analogous to well-known results for external flows around bodies in translational motion with velocity $-\mathbf{V}(t)$ or equivalently, by a change of reference frame, flows around bodies at rest with fluid velocity $\mathbf{V}(t)$ at infinity. We prefer to state the results in the latter body frame and we omit all proofs, referring to standard sources such as Batchelor,[31] Lighthill,[35] Wu,[36] Eyink[11] and the review of Biesheuvel and Hagmeijer.[12] The main object of interest here is the force acting on the fixed body B

$$\mathbf{F}(t) = \int_{\partial B} (-P\mathbf{n} + \rho\boldsymbol{\tau}_w)\, dA,$$

with $P = \rho p$ the thermodynamic pressure and with $\boldsymbol{\tau}_w = \nu\boldsymbol{\omega}\times\mathbf{n} = 2\nu\mathbf{S}\cdot\mathbf{n}$ the viscous skin friction. This force is of course related to fluid impulse $\mathbf{I}(t)$ by the well-known relation $\mathbf{F}(t) = -d\mathbf{I}/dt$. In the special case of potential flow satisfying the no-penetration b.c. $\partial\phi/\partial n = 0$ at the body surface ∂B, the force is given by

$$\mathbf{F}_\phi(t) = -\int_{\partial B} P_\phi \mathbf{n}\, dA,$$

and the impulse by

$$\mathbf{I}_\phi(t) = -\rho\int_{\partial B} \phi\mathbf{n}\, dA,$$

once again related by $\mathbf{F}_\phi(t) = -d\mathbf{I}_\phi/dt$. Thus,

$$\langle \mathbf{F}_\phi \rangle = 0,$$

which is the "generalized d'Alembert paradox" for bodies in non-uniform translational motion. As in the work of Huggins, Lighthill[35,37] and others[11,12] have proposed to divide the flow into the background potential flow fields $\mathbf{u}_\phi, p_\phi$ and the complementary rotational fields $\mathbf{u}_\omega = \mathbf{u} - \mathbf{u}_\phi, p_\omega = p - p_\phi$. The "effective force" imposed by rotational fluid motions is then

$$\mathbf{F}_\omega(t) = \int_{\partial B} (-P_\omega\mathbf{n} + \rho\boldsymbol{\tau}_w)\, dA,$$

and the impulse of the rotational flow is

$$\mathbf{I}_\omega(t) = \frac{1}{2}\left[\int_\Omega \mathbf{x}\times\boldsymbol{\omega}(\mathbf{x},t)\, dV + \int_{\partial B} \mathbf{x}\times(\mathbf{n}\times\mathbf{u}_\omega(\mathbf{x},t))\, dA\right],$$

so that $\mathbf{F}_\omega(t) = -d\mathbf{I}_\omega/dt$. Note that $\boldsymbol{\Gamma} = \mathbf{n}\times\mathbf{u}_\phi$ can be regarded as the strength vector of a surface vortex sheet of the potential flow $\mathbf{u}_\phi$ and since $\mathbf{n}\times\mathbf{u}_\omega = -\mathbf{n}\times\mathbf{u}_\phi$ on ∂B,

$$\mathbf{I}_\omega(t) = \frac{1}{2}\int_\Omega \mathbf{x}\times\boldsymbol{\omega}_a(\mathbf{x},t)\, dV,$$

where $\boldsymbol{\omega}_a$ is the so-called *additional vorticity*, with the surface vortex sheet removed. Note that generally $\langle\mathbf{F}_\omega(t)\rangle \neq \mathbf{0}$ because $\mathbf{I}_\omega(t)$ increases monotonically as the rotational wake grows in extent and its impulse is not bounded in time.

In the present context of external flow, the quantity analogous to the rate of pressure work (13) for channel flows is the power dissipated by the drag force

$$\mathscr{W} := \mathbf{F}(t)\cdot\mathbf{V}(t). \quad (26)$$

The force decomposition $\mathbf{F}(t) = \mathbf{F}_\phi(t) + \mathbf{F}_\omega(t)$ immediately implies a corresponding decomposition of the dissipated power $\mathscr{W}(t) = \mathscr{W}_\phi(t) + \mathscr{W}_\omega(t)$. However, since impulse $\mathbf{I}_\phi(t) = \mathbb{A}\cdot\mathbf{V}(t)$ with $\mathbb{A}$ a time-independent *added mass* tensor depending only on the shape of the body, it follows that $\mathscr{W}_\phi = \mathbf{F}_\phi(t)\cdot\mathbf{V}(t) = \frac{d}{dt}(\frac{1}{2}\mathbf{V}(t)\cdot\mathbb{A}\cdot\mathbf{V}(t))$ and thus

$$\langle\mathscr{W}_\phi\rangle = 0.$$

Just as before, there is no time-average power dissipated by the potential drag force and all of the "effective dissipation" arises from drag force due to rotational flow

$$\mathscr{W}_\omega := \mathbf{F}_\omega(t) \cdot \mathbf{V}(t). \tag{27}$$

It was shown by Eyink[11] that a detailed Josephson–Anderson relation holds for the latter, of the same form as (16)

$$\mathscr{W}_\omega = \mathscr{T},$$

where $\mathscr{T}$ is given by exactly the same expression (15). Thus, power dissipated by drag on the body due to rotational fluid motions is given instantaneously by the space integral of the vorticity flux across the flowlines of the background potential. In fact, this result is just a special case of a more general result of Howe,[13] which applies to arbitrary rigid body motion (translation and rotation) and which gives all force components, not only drag but also lateral forces such as lift.

It was pointed out by Eyink[11] that the JA-relation should hold even in the limit of infinite Reynolds number, if spatial integration-by-parts is performed to rewrite the transfer term in (15) instead as

$$\mathscr{T} = -\rho \int_\Omega \nabla \mathbf{u}_\phi : \mathbf{u}_\omega \mathbf{u}_\omega \, dV + \rho \int_\Omega \mathbf{u}_\phi \cdot \mathbf{f} \, dV + \rho \int_{\partial\Omega} \mathbf{u}_\phi \cdot \boldsymbol{\tau}_w \, dA. \tag{28}$$

This mathematical conjecture of an infinite-Re limit has been verified by Quan and Eyink[38] for the case of no body-force ($\mathbf{f} = \mathbf{0}$) in flow around a solid body, providing a new resolution of the famous paradox of d'Alembert[33,34] and connecting with the Onsager theory of "ideal turbulence."[39–41] To derive these conclusions for the limit $Re \to \infty$ it is crucial that the reference potential flow velocity must be infinitely differentiable or C^∞, which could indeed be proved for external flow as long as the body surface is correspondingly smooth.

III. A NEW DETAILED RELATION FOR STREAMWISE PERIODIC POISEUILLE FLOWS

The previous developments reviewed above suggest that vorticity flux accounts for wall drag with great generality, in many incompressible fluid flows of practical and theoretical interest, and that the JA relation can provide a novel vorticity-based perspective on drag reduction. Unfortunately, a difficulty occurs in the straightforward application of the original relation of Huggins[5] to classical turbulent flows through pipes and channels. In that case, the fields $\mathbf{u}_{in}$ and $\mathbf{u}_{out}$ that appear in the boundary conditions (7) for the reference potential flow are both x-slices of a very complex and rough turbulent velocity field. This means that $\mathbf{u}_\phi$ is generally also spatially complex and rough, inheriting those properties from its boundary conditions. This poses a serious problem for mathematical analysis of the infinite-Reynolds limit,[38] since the arguments involved depend crucially on the smoothness of the potential flow. Furthermore, this non-smoothness of $\mathbf{u}_{in}$ and $\mathbf{u}_{out}$ makes more demanding the numerical computation of $\mathbf{u}_\phi$. The corresponding problem does not appear in typical superfluid applications, since the vortex tangles in that case are generally confined well within the channel interior.

Another important issue is that numerical simulations of turbulent pipe and channel flows in classical fluids very frequently employ periodic boundary conditions in the streamwise direction as a computational convenience. The flow may be driven either with a fixed bulk velocity or as Poiseuille flow with a fixed pressure gradient. In the latter case, a standard choice is to use a non-periodic linear potential $Q_{nper} = -\gamma(t)x$, where x is taken as the streamwise direction and $\gamma(t)$ is the resultant streamwise gradient in the total pressure h, but with velocity $\mathbf{u}$ and static pressure p both periodic. This situation is of the type considered by Huggins[5] but with the ends of the channel periodically joined so that $S_{in} = S_{out}$. In this setting, the naive approach would be to mimic exactly the original derivation and take as reference field the Euler flow with potential ϕ solving Laplace's equation with Neumann boundary conditions (7), without regard for the fact that $\mathbf{u}_{in} = \mathbf{u}_{out}$. All of the analysis and results of Huggins[5] then carry over in this setting. However, there is a serious difficulty. The potential ϕ_N is uniquely specified (up to a spatial constant) by the Laplace problem with Neumann boundary conditions (7), and these conditions guarantee that $\mathbf{n} \cdot \mathbf{u}_{\phi,in} = \mathbf{n} \cdot \mathbf{u}_{\phi,out}$ so that $\mathbf{n} \cdot \mathbf{u}$ is x-periodic. However, in general, the components of $\mathbf{u}_\phi$ perpendicular to $\mathbf{n}$ need not be periodic. In fact, any such discontinuity corresponds to a vortex sheet in $\mathbf{u}_\phi$ at $S_{in} = S_{out}$ with strength $\boldsymbol{\Gamma} = \mathbf{n} \times (\mathbf{u}_{\phi,out} - \mathbf{u}_{\phi,in})$. Since the surface $S_{in} = S_{out}$ was arbitrary chosen and any x-cross section could be equally selected for the construction, this means that there is a vortex sheet in the interior of the periodic domain and $\mathbf{u}_\phi$ is not truly potential.

Both of these problems can be illustrated in the case of turbulent Poiseuille flow through a smooth plane-parallel channel, using data from the Johns Hopkins turbulence database (JHTDB)[42,43] which hosts data from a numerical simulation at $Re_\tau = 1000$ on a space domain $[0, 8\pi] \times [-1, 1] \times [0, 3\pi]$ with periodic b.c. in the streamwise x-direction and spanwise z-direction, but stick b.c. in the wall-normal y-direction. We have obtained Huggins's reference potential ϕ_N by solving numerically Laplace's equation with boundary conditions (7), using a second-order central-difference scheme. The streamlines of this potential for one time snapshot from the database are plotted in panel (a) of Fig. 2 and show spatially irregular behavior near in-flow at $x = 0$ and out-flow at $x = 8\pi$. The same irregularity is observed in the results for the wall-normal velocity component v_ϕ plotted in Fig. 3 at in-flow and out-flow. Even more seriously, this velocity component can be seen to be streamwise anti-periodic as is also the spanwise component w_ϕ (see supplementary materials, §I), both corresponding to a vortex sheet in $\mathbf{u}_\phi$. Interestingly, however, after inertial adjustment over a length of order the channel half-width, the potential flow field closely resembles a plug flow with spatially constant velocity $\mathbf{u}_\phi = U\hat{\mathbf{x}}$, for U the bulk flow velocity. The latter observation suggests that it might be possible in this case to use as reference flow the simple Euler

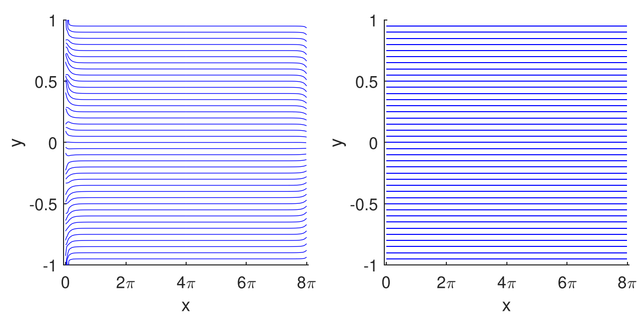

(a) Huggins' potential ϕ_N with Neumann b.c.

(b) Modified potential ϕ_M with mixed b.c.

FIG. 2. Streamlines of the reference potential for a snapshot of streamwise-periodic turbulent channel flow: (a) Huggins's potential φ_N with Neumann b.c. (b) Modified potential φ_M with mixed b.c.

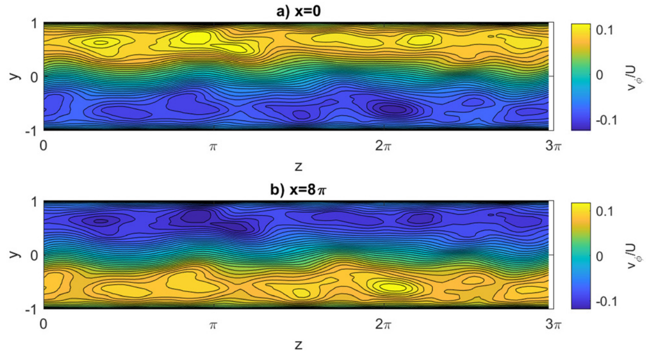

FIG. 3. Anti-periodic wall-normal component v_ϕ of Huggins's potential flow velocity for a snapshot of turbulent channel flow, at inflow $x = 0$ and outflow $x = 8\pi$. (a) $x = 0$. (b) $x = 8\pi$.

solution $\mathbf{u}_\phi = U\hat{\mathbf{x}}$ with non-periodic potential $\phi = Ux$, which has constant values $\phi = 0$ at $x = 0$ and $\phi = 8\pi U$ at $x = 8\pi$. This idea is readily verified.

Motivated by this example, however, we show here that one may more generally derive a Josephson–Anderson relation for streamwise-periodic Poiseuille flows using a modified potential ϕ_M satisfying Dirichlet b.c. at the end sections and which is periodic plus a linear part. We can consider generalized pipe and channel flows with curved or rippled walls, but, for technical reasons explained below, we must assume that the flow domain extends over $x \in [-0.5L_x, 0.5L_x]$ and S_{in}, S_{out} are flat surfaces of constant x-value. For the case of channels we assume likewise a spanwise extent $z \in [-0.5L_z, 0.5L_z]$, with periodic b.c. Finally, the flow is assumed driven by a non-periodic potential $Q_{nper} = -\gamma(t)x$, with fluid velocity $\mathbf{u}$ and static pressure p that are x-periodic. As we shall see, with these assumptions alone we may derive a version of the Kelvin minimum energy theorem. However, to derive the JA-relation and to guarantee that the potential flow velocity $\mathbf{u}_\phi$ is C^∞ on the torus we must require further that the flow domain is reflection-symmetric about the spanwise-wall normal midplane at $x = 0$, as shown in Fig. 4.[44] Additionally, at the intersection of the sidewalls S_w with inflow surface S_{in} and outflow surface S_{out} we assume that the normal vectors satisfy the geometric conditions,

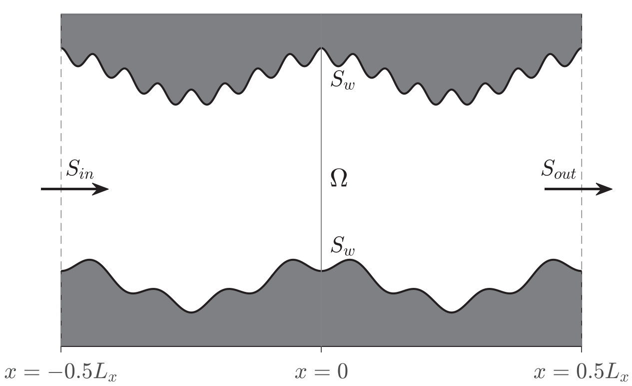

FIG. 4. Flow through a channel Ω with inflow surface S_{in}, outflow surface S_{out}, and sidewalls S_w. The domain is symmetric about the spanwise-wall normal plane at $x = 0$.

$$\mathbf{n}_w \cdot \mathbf{n}_{in} = \mathbf{n}_w \cdot \mathbf{n}_{out} = 0, \tag{29}$$

required for compatibility between Neumann conditions on S_w and Dirichlet conditions on S_{in} and S_{out}.

Under these assumptions we define the potential ϕ_M of the reference Euler solution to satisfy the Laplace equation, $\nabla^2\phi_M = 0$, with mixed Neumann–Dirichlet boundary conditions

$$\left.\frac{\partial\phi_M}{\partial n}\right|_{S_w} = 0, \quad \phi_M|_{S_{in}} = -\frac{1}{2}\Phi(t), \quad \phi_M|_{S_{out}} = +\frac{1}{2}\Phi(t). \tag{30}$$

For channel flow, we assume spanwise periodic boundary conditions as well. Here, the potential difference $\Phi(t)$ is chosen so that the Euler flow carries the entire mass flux, that is

$$J_\phi(t) := \rho\int_{S_{in}} \mathbf{u}_\phi \cdot \hat{\mathbf{n}}\, dA = \rho\int_{S_{out}} \mathbf{u}_\phi \cdot \mathbf{n}\, dA \tag{31}$$

$$= \rho\int_{S_{in}} \mathbf{u} \cdot \hat{\mathbf{n}}\, dA = \rho\int_{S_{out}} \mathbf{u} \cdot \mathbf{n}\, dA := J(t). \tag{32}$$

This potential is easily calculated by exploiting the homogeneity of the problem and first solving for $\phi_* = \phi_M/\Phi$, which satisfies the Laplace equation, $\nabla^2\phi_* = 0$ with mixed boundary conditions,

$$\left.\frac{\partial\phi_*}{\partial n}\right|_{S_w} = 0, \quad \phi_*|_{S_{in}} = -\frac{1}{2}, \quad \phi_*|_{S_{out}} = +\frac{1}{2}, \tag{33}$$

for which a unique solution exists. Now, let $\mathbf{u}_{\phi*} = \boldsymbol{\nabla}\phi_*$ and $J_* = \rho\int_{S_{in}} \mathbf{u}_{\phi*} \cdot \mathbf{n}\, dA$, leading to $J(t) = J_*\Phi(t)$ and

$$\phi_M = \Phi(t)\phi_* = J(t)\phi_*/J_*. \tag{34}$$

Observe that ϕ_* and consequently J_* depend only on the channel geometry. The potential $\phi_M(t)$ that results for given $J(t)$ is uniquely defined, although, in general, it may depend upon the arbitrary choice of the surface $S_{in} = S_{out}$ in the periodic domain Ω. We remark in passing also that $E_\phi = (1/2)J\,\Phi$, as shown by using as curvilinear coordinates the potential ϕ_M itself and any parameterization of ϕ_M-isosurfaces and by noting that $d\phi_M = |\mathbf{u}_\phi|d\ell$ for arc length ℓ along streamlines.

The above construction yields a reference Euler solution $\mathbf{u}_\phi$ which is C^∞ and x-periodic, when reflection symmetry of Ω about its midplane is assumed. Since $\bar{\phi}_M(x, y, z) := -\phi_M(-x, y, z)$ is another solution of the mixed boundary-value problem (30), uniqueness of that solution implies the symmetry property

$$\phi_M(-x, y, z) = -\phi_M(x, y, z). \tag{35}$$

This fact will be exploited together with the fact that the harmonic function $\phi_M \in C^\infty(\mathring{\Omega})$ where $\mathring{\Omega} = \Omega \backslash (S_{in} \cap S_{ou} \cap S_w)$ is the interior of the domain. See Ref. 45, Theorem 2.6, p. 28. Note that ϕ_M will, in general, be smooth up to S_w if the sidewall S_w is smooth, but we must show that all derivatives approaching $S_{in} = S_{out}$ from both sides agree. It is an elementary consequence of (35) that

$$\partial_x^m\phi_M\left(-\frac{L_x}{2}, y, z\right) = \partial_x^m\phi_M\left(+\frac{L_x}{2}, y, z\right), \quad \text{for all odd } m. \tag{36}$$

We next show by induction that

$$\partial_x^m\phi_M\left(-\frac{L_x}{2}, y, z\right) = \partial_x^m\phi_M\left(+\frac{L_x}{2}, y, z\right) = 0, \quad \text{for all even } m \geq 2. \tag{37}$$

For $m=2$, this follows by using the fact that ϕ_M is harmonic and is a spatial constant $\phi_M = \pm\Phi/2$ for $x = \pm L_x/2$, so that

$$\partial_x^2\phi_M\left(\pm\frac{L_x}{2}, y, z\right) = -(\partial_y^2 + \partial_z^2)\phi_M\left(\pm\frac{L_x}{2}, y, z\right) = 0.$$

We now assume that (37) holds for all even integers up to m and then note that

$$\partial_x^{m+2}\phi_M\left(\pm\frac{L_x}{2}, y, z\right) = -\partial_x^m(\partial_y^2 + \partial_z^2)\phi_M\left(\pm\frac{L_x}{2}, y, z\right) = 0,$$

by using the Laplace equation and the induction hypothesis, thereby completing the induction. It follows from (36) and (37) that $\mathbf{u}_\phi = \nabla\phi_M$ is both x-periodic and C^∞ in Ω.

Note that the velocity potential ϕ_M itself obviously cannot be periodic, because of the anti-periodic b.c. (30). On the other hand, it is not hard to show that $\phi_{per} := \phi_M - \Phi x/L_x$ is x-periodic. In fact, this function solves the Laplace equation $\nabla^2\phi_{per} = 0$ in Ω with the mixed boundary conditions

$$\frac{\partial\phi_{per}}{\partial n} = -\frac{\Phi}{L_x} n_x\Big|_{S_w}, \quad \phi_{per} = 0|_{S_{in}}, \quad \phi_{per} = 0|_{S_{out}}.$$

The solution of this problem is unique and x-periodic, vanishing on $S_{in} = S_{out}$. Furthermore, $\nabla\phi_{per} = \nabla\phi_M - \Phi/L_x$ so that the preceding discussion shows that ϕ_{per} is a C^∞ function on the entire flow domain Ω. We thus conclude that ϕ_M is the sum of a (smooth) periodic function and a function linear in x

$$\phi_M = \phi_{per} + \Phi x/L_x.$$

This fact will prove important in our derivation below.

With these results in hand, we can essentially repeat the construction of Huggins.[5] We note here just the key differences. One can define $\mathbf{u}_\omega = \mathbf{u} - \mathbf{u}_\phi$ as before, but now $\mathbf{u}_\omega$ satisfies the non-flow-through constraints (20) only at S_w and not at $S_{in} = S_{out}$. However, the condition (32) that $\mathbf{u}_\phi$ carries the total mass flux still yields the weaker result that

$$\int_{S_{in}} \mathbf{u}_\omega \cdot \hat{\mathbf{n}}\, dA = \int_{S_{out}} \mathbf{u}_\omega \cdot \mathbf{n}\, dA = 0. \tag{38}$$

This suffices to imply that the potential and vortical fields are orthogonal, as the following brief calculation shows:

$$\begin{aligned}\int_\Omega \mathbf{u}_\phi \cdot \mathbf{u}_\omega\, dV &= -\int_{S_{in}} \phi_M \mathbf{u}_\omega \cdot \mathbf{n}\, dA - \int_{S_{out}} \phi_M \mathbf{u}_\omega \cdot \mathbf{n}\, dA \\ &\quad - \int_{S_w} \phi_M \mathbf{u}_\omega \cdot \mathbf{n}\, dA \\ &= \frac{1}{2}\Phi(t)\int_{S_{in}} \mathbf{u}_\omega \cdot \mathbf{n}\, dA - \frac{1}{2}\Phi(t)\int_{S_{out}} \mathbf{u}_\omega \cdot \mathbf{n}\, dA = 0.\end{aligned} \tag{39}$$

Note that neither smoothness of ϕ_M nor even flatness of the sections S_{in}, S_{out} were required here. The other key step in the derivation of Huggins[5] where the constraints (20) were used was in the calculation (23) of the balance equation for E_ω, where they were invoked to eliminate the boundary terms at S_{in} and S_{out} involving h_ω. In fact, the weaker conditions (38) again suffice, if one recalls that

$$h_\omega = h + \partial_t\phi_M = p + \frac{1}{2}|\mathbf{u}|^2 + Q + \partial_t\phi_M, \tag{40}$$

so that h_ω is the sum of a smooth, x-periodic part $h_{\omega,per} = p + \frac{1}{2}|\mathbf{u}|^2 + Q_{per} + \partial_t\phi_{per}$ and a linear part $h_{\omega,lin} = \dot{\Phi}x/L_x - \gamma x$. In that case, the periodic part gives no contribution and the linear part contributes zero also because

$$\begin{aligned}\rho\int_{S_{in}} h_{\omega,lin}\mathbf{u}_\omega \cdot \mathbf{n}\, dA &+ \rho\int_{S_{out}} h_{\omega,lin}\mathbf{u}_\omega \cdot \mathbf{n}\, dA \\ &= -\frac{1}{2}(\dot{\Phi} - \gamma L_x)\rho\int_{S_{in}} \mathbf{u}_\omega \cdot \mathbf{n}\, dA \\ &\quad + \frac{1}{2}(\dot{\Phi} - \gamma L_x)\rho\int_{S_{out}} \mathbf{u}_\omega \cdot \mathbf{n}\, dA = 0.\end{aligned} \tag{41}$$

Here, we required flatness of S_{in}, S_{out} so that $h_{\omega,lin}$ is constant on those surfaces and continuity of $\mathbf{u}_\omega = \mathbf{u} - \mathbf{u}_\phi$ at $S_{in} = S_{out}$ to cancel the contribution from $h_{\omega,per}$. In conclusion, the balance equation (23) for E_ω again holds, and all of the rest of the derivation is identical to that of Ref. 5.

There are a few further simplifications compared with the construction of Huggins[5] due to the fact that both h and h_ω are now smooth, x-periodic functions plus a part which is linear in x. Thus, rate of work $\mathscr{W}$ by total pressure head defined in (13) now becomes

$$\mathscr{W} = \gamma(t)L_x J = (\Delta h)J,$$

where we have defined $\Delta h = \gamma L_x$ as the drop in total pressure. Likewise, the work done by the total rotational pressure is

$$\mathscr{W}_\omega = \left[(\Delta h) - \dot{\Phi}\right]J = (\Delta h_\omega)J,$$

so that the detailed JA-relation now becomes simply

$$\mathscr{T} = (\Delta h_\omega)J = (\Delta h)J - \mathscr{W}_\phi. \tag{42}$$

The rate of work by the potential flow simplifies also as

$$\mathscr{W}_\phi = J\dot{\Phi} = J\dot{J}/J_* = \dot{E}_\phi. \tag{43}$$

For the special case of a flow with a mass flux constant in time, $dJ/dt = 0$, one gets furthermore $\Delta h_\omega = \Delta h$ and $\mathscr{T} = (\Delta h)J$.

It is also instructive to consider the canonical case of channel flow with flat plane-parallel walls and $\mathbf{f} = \mathbf{0}$. In that case, as previously noted, our construction yields $\phi_M(t) = U(t)x$ and $\mathbf{u}_\phi = U(t)\hat{\mathbf{x}}$ is spatially constant. It follows then from the alternative formula (28) for $\mathscr{T}$ in the Introduction that

$$\mathscr{T} = \rho U\int_{S_w} \tau_{xy}^w\, dA, \tag{44}$$

which is the energy dissipated by viscous wall drag. Thus, in this particular case, both the work done against rotational pressure and the dissipation by drag are instantaneously related to vorticity flux across the channel. The transfer term likewise simplifies to

$$\mathscr{T} = -\rho U\int_\Omega \Sigma_{yz}\, dV = -\rho U\int_\Omega (\omega_z v - \omega_y w - \nu\partial_y\omega_z)\, dV,$$

where note that $\int_\Omega \partial_z\omega_y\, dV = 0$ because of the spanwise periodic b.c. Note further because of the vector calculus identity,

$$\omega_z v - \omega_y w = -\partial_x(u^2) - \partial_y(vu) - \partial_z(wu) + \frac{1}{2}\partial_x(u^2 + v^2 + w^2), \tag{45}$$

and the assumed boundary conditions, the net contribution to $\mathscr{T}$ from the nonlinear term *vanishes*, when integrated over the flow volume. This vanishing value is special to channel flow with flat, parallel walls, because of the high degree of symmetry of this flow, whereas the nonlinear contribution to the JA-relation is generally not zero (e.g., see Sec. IV). Integrating the remaining term $\nu\partial_y\omega_z$ in y directly recovers (44) and the detailed JA-relation reduces to an instantaneous version of the time-average result for turbulent channel flow, $\langle\Sigma_{yz}\rangle = -u_\tau^2/h$, previously discussed in the literature.[8,14,15] Note, however, that the time-average $\langle\omega_z v - \omega_y w\rangle(y) \neq 0$ and this term is crucial to give a y-independent constant mean total flux, although contributions from negative and positive signs of the mean nonlinear flux exactly cancel when integrated over y-locations. See Ref. 15 for more discussion of the physical mechanisms.

IV. NUMERICAL RESULTS FOR A FLAT-WALL CHANNEL WITH A SMOOTH BUMP

In this section, we present a numerical application of our new detailed JA relation. In order to investigate flow separation and its contribution to drag, we have selected for study a streamwise-periodic channel flow with plane-parallel walls modified by addition of a smooth bump or ridge at the wall, with a cosine profile in the streamwise direction over a complete period, from minimum to minimum, and spanwise constant. The shape is given by the bump function

$$b(x) = \begin{cases} \frac{1}{2}h\,(1+\cos(2\pi(x-c)/\ell)) & |x-c| \le \ell/2, \\ 0 & \text{otherwise,} \end{cases}$$

expressing elevation above the bottom wall, centered at $x = c$, with length ℓ and height h. See Fig. 5 for a sideview of the geometry. We keep the bulk flow velocity U constant, for ease of demonstration, with the pressure gradient $\gamma(t)$ which drives the flow varying to maintain the constant flow rate. We take the x-direction as streamwise, y-direction as wall-normal and z-direction as spanwise. We consider a domain of size $(L_x, L_y, L_z) = (1, 1, 0.5)$ in arbitrary units and for the cosine bump we take $c = \ell = 0.5L_x$ and $h = 0.1L_x$. We initialize the velocity field with a constant value $\mathbf{u} = (U, 0, 0)$, The Reynolds number based on bulk velocity U and channel height L_y is thus constant at $Re = UL_y/\nu = 975$, which results in an unsteady laminar flow, sufficient to drive flow separation from the bump and to generate a rotational wake.

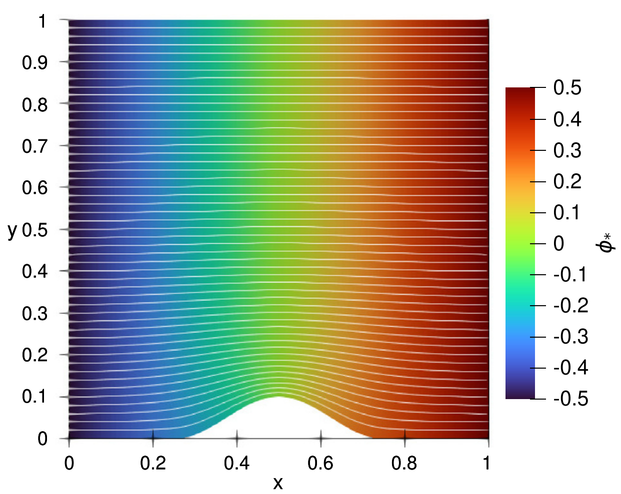

FIG. 5. Dimensionless background potential ϕ_* and its streamlines.

To compute this flow numerically, we use the laminar pimpleFoam[46] solver from OpenFOAM,[47] with a body-fitted structured mesh of hexahedral cells and a range of mesh sizes listed in Table I. A convergence study shows that the results are accurate within a few percent for the finest mesh $(N_x, N_y, N_z) = (216, 216, 108)$ (see below) and all concrete results presented here are for that resolution. Numerical field values are output at time intervals of $\Delta tU/L_x = 0.195$ starting at $tU/L_x = 0.195$. Our goal is to numerically evaluate the detailed JA-relation (42), which here takes the concrete form

$$\gamma(t)L_x J = -\int_\Omega \rho\mathbf{u}_\phi \cdot (\mathbf{u}\times\boldsymbol{\omega} - \nu\nabla\times\boldsymbol{\omega})\,dV := \mathscr{T}(t), \tag{46}$$

since $dJ/dt = 0$ and $\mathbf{f} = \mathbf{0}$. The volume-integral in (46) was computed numerically by a Riemann sum where each cell is associated with a single value and all values are multiplied by cell volume and added to get integrals. To obtain $\mathbf{u}_\phi = \Phi(t)\mathbf{u}_\phi^*$, the geometry-dependent dimensionless potential ϕ_* satisfying b.c. (33) was calculated by solving the Laplace equation using laplacianFoam. This solver uses the conjugate gradient method to solve the linear system that results from the same structured mesh of hexahedral cells used to discretize Navier–Stokes. The results are shown in Fig. 5, which plots ϕ_* as a color map and representative streamlines. The prefactor $\Phi(t)$ is time-independent for this flow with constant bulk velocity and fixed by the relation $\Phi = J/J_*$. All space-gradients such as $\boldsymbol{\omega} = \nabla\times\mathbf{u}$ and $\nabla\times\boldsymbol{\omega}$ were calculated by central differences. We find that the maximum relative error between the left-hand side (LHS) and right-hand side (RHS) of the JA relation (46), or $RelErr(\%) = 100\max_t|1 - \frac{\mathscr{T}(t)}{JL_x\gamma(t)}|$ decreases with mesh resolution, as shown in the final column of Table I. We deemed the maximum error $\leq 3.56\%$ achieved at our highest resolution to be adequate for the purposes of this study.

More detailed information about accuracy is afforded by the plots in Fig. 6 of the time series of the driving pressure-gradient $\gamma(t)$ and of the transfer term $\mathscr{T}(t)$ in the detailed JA-relation, suitably nondimensionalized, which agree quite well over the entire recorded time period. However, in addition to numerical validation, further information about the physics is provided by the plots in Fig. 6 of the separate contributions to $\mathscr{T}(t)$ arising from viscous and nonlinear vorticity transport. At the moderate Reynolds number of the simulation, the

TABLE I. The effect of grid size on maximum error.

Case	Nx	Ny	Nz	$RelErr(\%)$
1	50	50	25	11.7
2	80	80	40	7.88
3	160	160	81	4.38
4	216	216	108	3.56

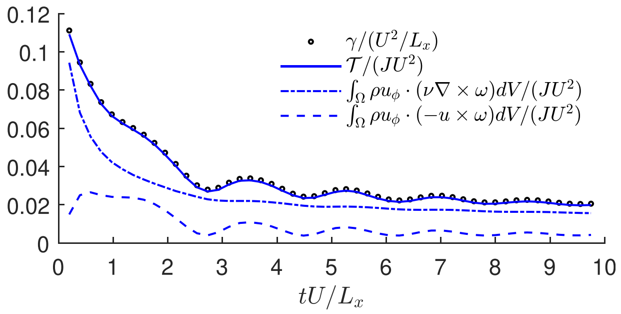

FIG. 6. Time series of terms in the detailed JA relation [Eq. (46)] for flow past a bump in a periodic channel with a constant flow rate ($dJ/dt = 0$), also showing separate viscous and nonlinear contributions to the transfer term.

viscous contribution is largest and the nonlinear contribution only about half as large. On the other hand, the instantaneous drag as measured by $\gamma(t)$ exhibits distinctive oscillations, which are contributed entirely by the nonlinear transport term in $\mathscr{T}(t)$ whereas the viscous term decays monotonically in time. We argue that the local maxima in drag are due to periodic episodes of strong vortex shedding from the smooth bump, whereas the local minima are due to episodes of weaker shedding. We present several pieces of evidence to support this interpretation.

One such piece of evidence comes from an additional exact relation derived from the constraint $\frac{1}{L_xL_yL_z}\int_\Omega \mathbf{u}\, dV = U\hat{\mathbf{x}}$ and the global momentum balance obtained by integrating the governing Navier–Stokes equation over the flow domain

$$\int_{S_w} (-P\mathbf{n} + \rho\boldsymbol{\tau}_w)\, dA + \dot{J}(t)L_x = \rho\gamma(t)L_xL_yL_z\hat{\mathbf{x}}. \tag{47}$$

In the case considered here $dJ/dt = 0$, so that global momentum balance reduces to the relation

$$\mathbf{F}(t) := \int_{S_w} (-P\mathbf{n} + \rho\boldsymbol{\tau}_w)\, dA = \rho\gamma(t)L_xL_yL_z\hat{\mathbf{x}}, \tag{48}$$

where the left-hand side is the instantaneous drag force exerted by the fluid on the channel walls and the right-hand side is the instantaneous force applied by the external pressure gradient to the fluid. Plotted in

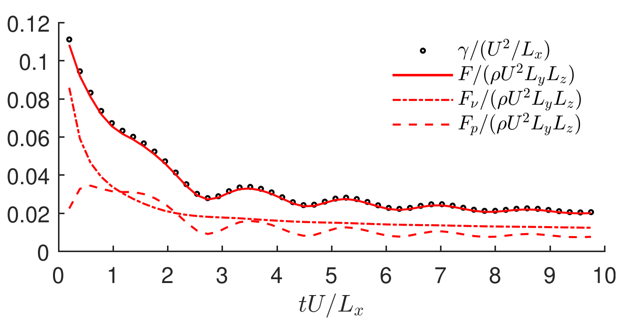

FIG. 7. Time series of terms in the global momentum balance, the net drag force $F_x(t)$ on the wall and the instantaneous pressure gradient $\gamma(t)$, also showing separate contributions from skin friction and pressure to drag force.

Fig. 7 are the times series of the x-components of the two sides of Eq. (48), suitably normalized, whose excellent agreement again validates our numerical solution. More physically informative are the plots in Fig. 7 of the separate contributions to the drag force from the viscous skin friction and the pressure (form drag), which show remarkably similar (but not identical) behaviors as the viscous and nonlinear transport contributions to the JA-relation as plotted in Fig. 6. The similarity of the viscous contributions is unsurprising, as we have already noted in Eq. (28) that

$$\int_\Omega \mathbf{u}_\phi \cdot \nu\boldsymbol{\nabla} \times \boldsymbol{\omega}\, dV = \int_{\partial\Omega} \mathbf{u}_\phi \cdot \boldsymbol{\tau}_w\, dA, \tag{49}$$

by a simple application of the divergence theorem. Thus, the viscous term in the JA transfer term coincides with the viscous term in the drag force after substituting $\mathbf{u}_\phi$ for $U\hat{\mathbf{x}}$. Since Fig. 5 shows that $\mathbf{u}_\phi$ and $U\hat{\mathbf{x}}$ are quite similar, it is understandable that the two viscous contributions are closely correlated.

We cannot find any such direct correspondence between the nonlinear term $\mathscr{T}_{nlin}(t)$ and the form drag $F_{px}(t)$, but it is well known that large form drag is associated with earlier or stronger shedding of vorticity by flow separation. Thus, the similar oscillations observed in both the form drag and the nonlinear transfer term are likely both due to oscillations in separation. Boundary-layer separation can, in fact, be verified in this flow by visualization of spatial fields in Fig. 8. For simplicity we have chosen to visualize a late time $tU/L_x = 9.75$ when the flow has become nearly steady and we plot fields in the vertical xy-plane at the spanwise midsection $z = 0.25$. The plot of the streamwise velocity u in Fig. 8(a) is relatively uninformative, showing just a slightly elevated region of reduced streamwise velocity downstream of the bump. However, the plot of the wall-normal velocity v in Fig. 8(b) shows a clear upward jet just upstream of the bump, while just downstream there is a bipolar pattern of downflow followed by upflow indicative of a recirculation bubble. Most compelling is the plot of the spanwise vorticity in Fig. 8(c), which shows a strong sheet of negative spanwise vorticity on the upstream face of the bump associated with a viscous boundary layer which is then shed into the flow downstream of the bump. On the downstream face of the bump, the vorticity is instead positive, indicating a recirculation bubble. In fact, we see such clear evidence of flow separation at all recorded times.

To get a physical understanding of the relation of drag to such vorticity dynamics, we can visualize the integrand appearing in the spatial integral which defines the transfer term $\mathscr{T}(t)$ in the detailed JA-relation of Eq. (46). We plot this integrand in Fig. 9 at the same time $tU/L_x = 9.75$ and in the xy-plane at the same spanwise position $z = 0.25$ as the flow fields plotted in Fig. 8, so that the two may be compared directly. We note, however, that while our flow varies substantially in time, it is rather spanwise homogeneous, so that the plots in xy-planes at other spanwise positions are very similar. We plot in Fig. 9(a) the viscous contribution to the integrand, in Fig. 9(b) the nonlinear contribution, and in Fig. 9(c) the combined integrand, representing local total flux of vorticity across flowlines of the Euler potential. We discuss each of the plots in turn.

The viscous contribution to the JA-transfer term plotted in Fig. 9(a) can be readily understood, because Huggins's flux tensor $\boldsymbol{\Sigma}$ appearing in (15) for flux normal to the wall is exactly equal to the Lighthill boundary vorticity source $\boldsymbol{\sigma}$, or

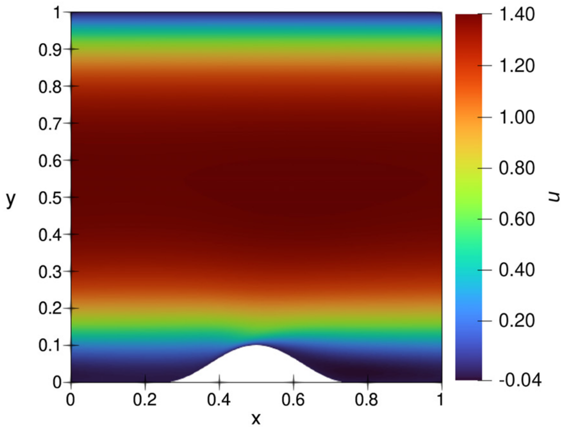

(a) Streamwise velocity

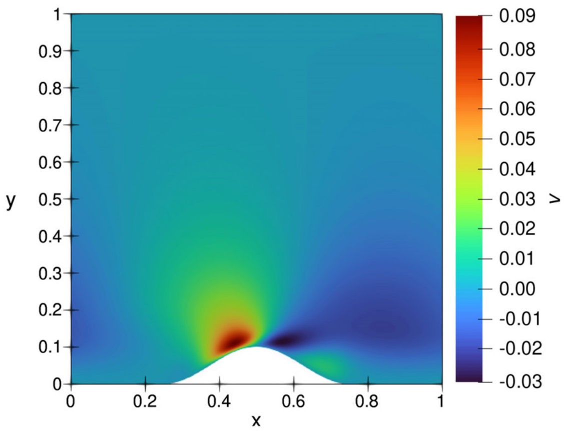

(b) Wall-normal velocity

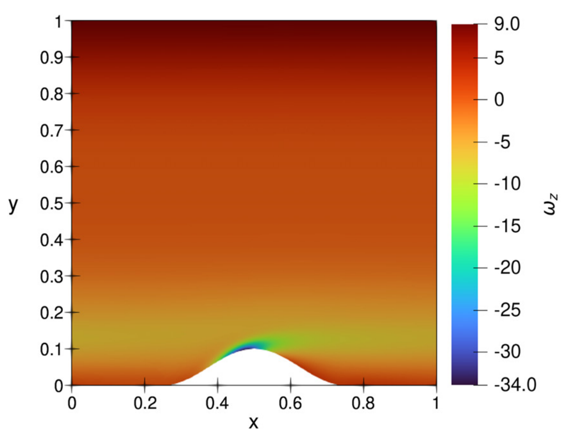

(c) Spanwise vorticity

FIG. 8. Instantaneous velocity fields, (a) streamwise and (b) wall-normal, normalized by U, and (c) spanwise vorticity field normalized by U/L_x, at $tU/L_x = 9.75$, $z = 0.25$.

$$\boldsymbol{\Sigma}^\top \mathbf{n} = \boldsymbol{\sigma} = \nu \mathbf{n} \times (\boldsymbol{\nabla} \times \boldsymbol{\omega}), \tag{50}$$

where the relevant expression for $\boldsymbol{\sigma}$ is that of Lyman[48] rather than the alternative expression of Lighthill[10] and Panton.[49] Thus, the viscous vorticity flux in the flow interior directly continues that from the solid wall. Crucially, all transfer terms plotted in Fig. 9 arise from *wall-normal flux of spanwise vorticity*, since the potential flow-lines are parallel to the wall and furthermore $\boldsymbol{\omega} \cdot \mathbf{n} = 0$ and $\mathbf{n} \cdot \boldsymbol{\sigma} = 0$, i.e., wall-normal vorticity and its fluxes are negligible in the vicinity of the surface. However, as also emphasized by Lighthill[10] and especially by Morton,[50] vorticity generation at the surface is an essentially inviscid process driven by tangential pressure gradients, as shown by the equivalent formula

$$\boldsymbol{\sigma} = -\mathbf{n} \times \boldsymbol{\nabla} p. \tag{51}$$

Thus, the favorable pressure-gradient on the upstream side of the bump generates negative spanwise vorticity, whereas the adverse pressure-gradient on the downstream side generates positive spanwise vorticity. For plots of the pressure fields, see supplementary material, Sec. IV. These signs are observed both in the plot of spanwise vorticity in Fig. 8(c) and in the plot of the viscous transfer in Fig. 9(a). As emphasized by Lighthill,[10] however, the change of sign of σ_z occurs earlier than the change of sign of ω_z (the point of separation), because it takes some time for the reversed positive flux to subtract the negative vorticity already present, and this delay is clearly observed in Figs. 8(c) and 9(a). The viscous transport of spanwise vorticity into the flow interior continues that at the surface but decreases rapidly as vorticity gradients drop off.

The nonlinear contribution to the JA-transfer term plotted in Fig. 9(b) is the dominant one through the bulk of the flow, but consists of two large lobes of opposite sign upstream and downstream of the bump, which substantially cancel. Thus, at the moderate Reynolds number of this simulation, nonlinear transfer provides only 21.4% to the instantaneous drag at $tU/L_x = 9.75$ and viscous transfer the remaining 78.6%. The dominant contribution to the nonlinear vorticity flux in the region above the bump is the streamwise advection of spanwise vorticity, $\Sigma_{xz} \simeq u\omega_z$, as may be seen from the plots in Fig. 8. The streamwise velocity plotted in Fig. 8(a) is more than an order of magnitude larger than the wall-normal component in Fig. 8(b), while the spanwise velocity (not shown) is even smaller. The largest component of vorticity is by far the spanwise one ω_z and, in the region just above the bump, its sign is negative. This is the dominant sign of vorticity shed from the bump which then, given the periodic boundary conditions, recirculates through the domain in the streamwise direction. Note, incidentally, that the dominant shedding of negative spanwise vorticity is directly related to form drag on the bump by the Lighthill–Morton relation (51), since the smaller flux of positive vorticity after separation implies that the pressure never fully recovers its upstream value. The flux Σ_{xz} contributes to transfer across the potential streamlines because the latter bend vertically upward just upstream of the bump and vertically downward just downstream; see Fig. 5. These considerations easily account for the observed signs of the two lobes in Fig. 9(b).[51] The reason that the positive/drag-producing lobe downstream dominates over the negative/drag-reducing lobe upstream is that the streamwise vorticity is strongest immediately after it is shed, whereas the vorticity periodically reentering the flow domain upstream is diffused and weaker.

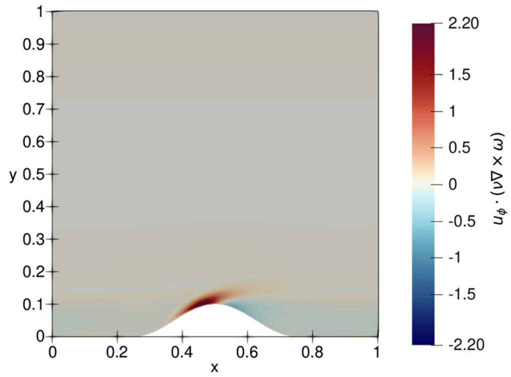

(a) Viscous contribution to $\mathscr{T}$-integrand, accounting for 78.6% of instantaneous drag.

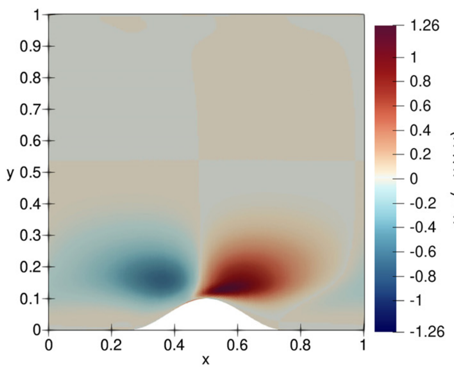

(b) Nonlinear contribution to $\mathscr{T}$-integrand, accounting for 21.4% of instantaneous drag.

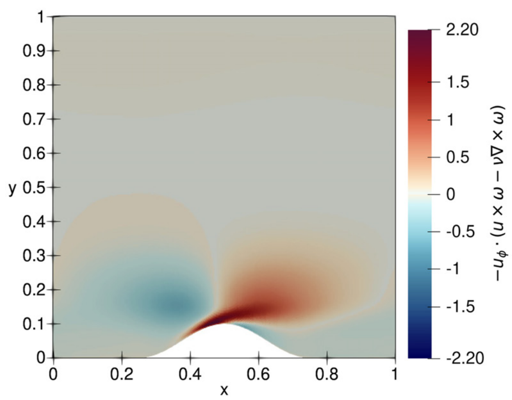

(c) $\mathscr{T}$-integrand in Eq. (46), representing local flux of spanwise vorticity across potential flowlines.

FIG. 9. Instantaneous fields of (c) the integrand of $\mathscr{T}$ in the detailed JA-relation (46), and (a) viscous and (b) nonlinear contributions to the integrand, all normalized by $\rho U^3/L_x$. Fields are shown for $tU/L_x = 9.75$, $z = 0.25$. (a) Viscous contribution to T-integrand, accounting for 78.6% of instantaneous drag. (b) Nonlinear contribution to T-integrand, accounting for 21.4% of instantaneous drag. (c) T-integrand in Eq. (46), representing local flux of spanwise vorticity across potential flowlines.

Combining the viscous and nonlinear contributions yields the total transfer integrand plotted in Fig. 9(c). A very simple and intuitive picture thereby emerges for the origin of drag via vorticity dynamics. Negative spanwise vorticity is generated by the favorable pressure gradient on the upstream side of the bump, while a smaller amount of positive vorticity is generated by the adverse pressure gradient downstream. This vorticity viscously diffuses into the flow interior where nonlinear advection then takes over, convecting the excess negative spanwise vorticity downstream. Drag is produced as the negative spanwise vorticity crosses the streamlines of the background Euler potential. This picture directly relates the nonlinear flux contribution in the JA-relation to form drag, since the latter results from the shedding of excess negative spanwise vorticity, and we can therefore understand the high correlation between the two terms observed in Figs. 6 and 7. Note that the results that we have observed here for $tU/L_x = 9.75$ are quite general and hold at all recorded times. Only the strength of vortex shedding varies with time, with strong shedding at times of local maximum drag in Figs. 6 and 7 and weak shedding at times of local minimum drag. See Supplemental Material, Secs. II and III, in particular, for a comparison of the two times $tU/L_x = 3.51$ and $tU/L_x = 4.485$ corresponding to a local maximum and minimum, respectively.

Although we have considered only a single flow geometry at a single Reynolds number, many of our conclusions are much more general. In fact, the JA-relation has recently been evaluated by Du and Zaki[52] for external flow past spherical and spheroidal bodies and their results are very similar to ours. Spanwise (azimuthal) vorticity is generated in that flow principally by favorable pressure gradients on the body surface. This azimuthal vorticity diffuses outward from the sphere by viscosity but is shed rapidly into the flow by boundary-layer separation. Nonlinear advection takes over, with convection, stretching, and twisting of vorticity, and resultant drag is produced by the integrated flux of the azimuthal vorticity across the streamlines of the background Euler potential. One difference is that Du and Zaki[52] do not see an "anti-drag" lobe upstream of the body similar to ours in Fig. 9(c), because they do not use periodic boundary conditions and their inflow has negligible vorticity. In addition, their simulations are at higher Reynolds numbers than ours and the wake behind their body is fully turbulent. The vorticity dynamics in wall-bounded turbulent flows is more complex than what we observe in our laminar flow. As just one example, we observe nonlinear vorticity transfer in our flow to be dominated by streamwise advection of spanwise vorticity across potential streamlines, but the spanwise transport of wall-normal vorticity is found to play an essential role in turbulent channel-flow in the buffer layer and throughout the log-layer, related to velocity-correlated vortex-stretching.[15] Nevertheless, the drag in turbulent wall-bounded flows is due also to the cross-stream flux of spanwise vorticity.[8,14,15] Thus, the Josephson–Anderson relation reveals a deep underlying unity in the origin of drag via vorticity dynamics, encompassing flows both internal and external, both laminar and turbulent, and both classical and quantum.

V. CONCLUSIONS

We have reviewed in this paper the detailed Josephson–Anderson relation for instantaneous drag first derived by Huggins[5] for internal flows through general channels and we have explained how this result provides the exact analogue of the drag formulas for external flow past bodies derived by Wu,[36] Lighthill,[35,37] Howe,[13] Eyink,[11] and others.[12] In all of these works, instantaneous drag is divided into a potential part and an "effective" rotational part that arises from vorticity flux across streamlines of the background potential Euler flow. However, we showed that the original relation of Huggins[5] suffers from significant problems when applied to classical turbulence and, in particular, his prescription for the background potential introduces a spurious vortex sheet for the streamwise periodic flows that are widely employed in numerical simulations. We proposed instead a reference potential Euler flow whose mass flux matches that of the total velocity field, while also ensuring that the vortical and potential velocity fields are orthogonal. The main theoretical result of our paper is the new detailed Josephson–Anderson relation (42) for streamwise periodic flows, which equates the instantaneous rate of work $\mathscr{W}_\omega$ due to rotational pressure, given by (14), and the integrated flux of vorticity $\mathscr{T}$ across potential streamlines, given by (15). We finally illustrated the utility of this relation by the example of Poiseuille flow in a flat-wall channel with a single smooth bump at the wall. The main physical conclusion of our work is contained in the numerical results plotted in Fig. 9 and the resulting explanation of the origin of drag in terms of vorticity shed due to flow separation from the bump.

It is interesting to ask how our results are related to the views of Feynman on the role of vortex reconnections in superfluid turbulence. Posing the question "What can eventually become of the kinetic energy of the vortex lines?," Feynman[19] argued that "the lines (which are under tension) may snap together and join connections a new way" and he proposed a picture of a sequence of reconnections as a path to dissipation of vortex energy into elementary excitations. A modern version of this picture is the Kelvin wave cascade generated by vortex reconnections.[53,54] In fact, the experiments of Bewley *et al.*[16] and Fonda, Sreenivasan, and Lathrop[17,18] have visualized the quantized vortex lines in superfluid turbulence and observed their reconnection dynamics. We agree with the view that vortex reconnection is an intrinsic part of turbulence, not only in quantum fluids but also in classical fluids. A major difference is that classical vorticity distributions are continuous and Newtonian viscosity allows vorticity to diffuse like smoke through the fluid. However, the stochastic Lagrangian description of classical vortex motion via a Feynman–Kac representation shows that line-reconnection occurs everywhere in classical turbulent flows, continuously in time.[55–57] On the other hand, focusing on the small-scale dissipation of fluid-mechanical vortex motions into heat, in our opinion, misses another essential element of turbulent dissipation. Referring to classical fluid turbulence driven by a pressure gradient, Feynman[19] argued that "The vortex lines twist about in an ever more complex fashion, increasing their length at the expense of the kinetic energy of the main stream." In fact, complex, irregular motion is not sufficient to explain turbulent dissipation in such flows. The essential new idea supplied by Josephson[3] and Anderson,[4] which was missed by Feynman, is that organized *cross-stream vortex motion* and not just random stretching and reconnection is required to explain the enhanced energy dissipation in wall-bounded turbulence of both quantum and classical fluids.

In our opinion, this point is likely of key importance in the explanation of the *anomalous energy dissipation* for incompressible fluid turbulence, which was proposed by Onsager[39–41] and which was the subject of pioneering empirical investigations by Sreenivasan[25,26] and Meneveau and Sreenivasan.[27] Various experiments[58,59] have shown that the presence of wall-roughness is crucial for the existence of a dissipative anomaly and some phenomenological scaling theories[60,61] lead to the same conclusion. Experimental visualizations of flow around individual cubic roughness elements in a turbulent duct flow[62] exhibit similar features as our smooth bump, with form drag, flow separation and vortex shedding into the interior. It thus seems likely that such phenomena must persist in order to produce a dissipative anomaly in the infinite Reynolds number limit. It is known from experimental studies of Sreenivasan[20] and Sreenivasan and Sahay[21] that viscous effects persist in the log-layer of smooth-wall turbulent flows up to the location of peak Reynolds stress and mean vorticity flux, in particular, is dominated by viscous transport over this range.[8,15] Mathematical analysis[38,41,63] shows that anomalous viscous transport of vorticity outward from the wall may, in fact, persist in the infinite-Reynolds limit, and persistent shedding of vorticity and resultant form drag seem the most plausible mechanism for anomalous energy dissipation in rough-walled turbulent flows.

In future work, we hope to apply our new detailed Josephson–Anderson relation to several problems of current interest. Our work gives a new perspective on the problem of turbulent drag reduction which we plan to pursue, in particular, for polymer additives.[64] Note that the polymer stress contributes simply a body force $\mathbf{f} = \boldsymbol{\nabla}\cdot\boldsymbol{\tau}_p$ in the Navier–Stokes equation (1) and the detailed JA-relation hence applies directly to viscoelastic fluids. Another problem of practical importance is the parameterization of surface drag in rough-walled turbulent flows, which has already been investigated[65] by the Force Partition Method (FPM)[66,67] which is closely related to the Josephson–Anderson relation. The relationship of these two approaches deserves to be discussed at length, but we just note here that FPM derives an exact expression for form drag as a spatial integral of the second-order invariant $Q = -(1/2)\mathrm{Tr}\left[(\boldsymbol{\nabla}\mathbf{u})^2\right]$ and the viscous acceleration $\nu\Delta\mathbf{u}$ weighted by a scalar potential ϕ and its gradient $\boldsymbol{\nabla}\phi$, respectively. While such an integral relation is similar in form to the JA relation, FPM uses a different potential, yields results for the pressure contribution to drag only, and has the aim to relate form drag to Q-structures rather than to vorticity dynamics. Another approach to derive exact formulas for skin friction is that of Fukagata, Iwamoto, and Kasagi,[68] yielding the so-called FIK identity, and a vorticity-based version, in particular, relates the skin friction to velocity–vorticity correlations,[69] similar to the JA-relation. However, FIK-type identities apply only to flat-walled flows without form drag and yield a result only for homogeneous averages. The detailed Josephson–Anderson relation derived by Huggins[5] and extended in this work, by contrast, describes the total drag from both skin friction and form drag and applies instantaneously in time.

SUPPLEMENTARY MATERIAL

See the supplementary material for the following additional data that are available:

I. *Huggins's potential flow*: Spanwise and streamwise velocities, analogous to the wall-normal component in Fig. 3.
II. *Velocity and vorticity fields*: Plots analogous to Fig. 8 at times of a local maximum and local minimum of drag.
III. *JA transfer integrands*: Plots analogous to Fig. 9 at times of a local maximum and local minimum of drag.
Pressure fields: Comparison of potential Euler pressure and pressure at an early time; pressure at a drag maximum, drag minimum, and at the instant in Figs. 8 and 9.

ACKNOWLEDGMENTS

We thank Y. Du, N. Goldenfeld, J. Katz, C. Meneveau, R. Mittal, and T. Zaki for discussions of this problem and of their related results. We wish to express our gratitude to K. R. Sreenivasan for his friendship over many years and for his leadership in science, which we hope will continue well into the future. Finally, we thank the Simons Foundation for support of this work through the Targeted Grant No. MPS-663054, "Revisiting the Turbulence Problem Using Statistical Mechanics" and also the Collaboration Grant No. MPS-1151713, "Wave Turbulence."

AUTHOR DECLARATIONS

Conflict of Interest

The authors have no conflicts to disclose.

Author Contributions

Samvit Kumar: Conceptualization (equal); Data curation (lead); Formal analysis (equal); Funding acquisition (lead); Investigation (equal); Methodology (equal); Project administration (lead); Resources (equal); Supervision (lead); Validation (equal); Visualization (lead); Writing – original draft (equal); Writing – review & editing (equal). **Gregory L. Eyink:** Conceptualization (equal); Data curation (supporting); Formal analysis (equal); Funding acquisition (lead); Investigation (equal); Methodology (equal); Project administration (lead); Resources (equal); Supervision (lead); Validation (equal); Visualization (lead); Writing – original draft (equal); Writing – review & editing (equal).

DATA AVAILABILITY

The data that support the findings of this study are available from the corresponding authors upon reasonable request.

REFERENCES

[1]R. E. Packard, "The role of the Josephson-Anderson equation in superfluid helium," Rev. Mod. Phys. **70**, 641 (1998).
[2]E. Varoquaux, "Anderson's considerations on the flow of superfluid helium: Some offshoots," Rev. Mod. Phys. **87**, 803 (2015).
[3]B. D. Josephson, "Potential differences in the mixed state of type II superconductors," Phys. Lett. **16**, 242–243 (1965).
[4]P. W. Anderson, "Considerations on the flow of superfluid helium," Rev. Mod. Phys. **38**, 298–310 (1966).
[5]E. R. Huggins, "Energy-dissipation theorem and detailed Josephson equation for ideal incompressible fluids," Phys. Rev. A **1**, 332–337 (1970).
[6]W.-K. Kwok, U. Welp, A. Glatz, A. E. Koshelev, K. J. Kihlstrom, and G. W. Crabtree, "Vortices in high-performance high-temperature superconductors," Rep. Prog. Phys. **79**, 116501 (2016).
[7]A. Glatz, I. A. Sadovskyy, U. Welp, W.-K. Kwok, and G. W. Crabtree, "The quest for high critical current in applied high-temperature superconductors," J. Supercond. Novel Magn. **33**, 127–141 (2020).
[8]G. L. Eyink, "Turbulent flow in pipes and channels as cross-stream 'inverse cascades' of vorticity," Phys. Fluids **20**, 125101 (2008).
[9]G. I. Taylor, "The transport of vorticity and heat through fluids in turbulent motion," Proc. R. Soc. London, Ser. A **135**, 685–702 (1932).
[10]M. J. Lighthill, "Introduction: Boundary layer theory," in *Laminar Boundary Theory*, edited by L. Rosenhead (Oxford University Press, Oxford, 1963), pp. 46–113.
[11]G. L. Eyink, "Josephson-Anderson relation and the classical D'Alembert paradox," Phys. Rev. X **11**, 031054 (2021).
[12]A. Biesheuvel and R. Hagmeijer, "On the force on a body moving in a fluid," Fluid Dyn. Res. **38**, 716 (2006).
[13]M. S. Howe, "On the force and moment on a body in an incompressible fluid, with application to rigid bodies and bubbles at high and low Reynolds numbers," Q. J. Mech. Appl. Math. **48**, 401–426 (1995).
[14]E. R. Huggins, "Vortex currents in turbulent superfluid and classical fluid channel flow, the Magnus effect, and Goldstone boson fields," J. Low Temp. Phys. **96**, 317–346 (1994).
[15]S. Kumar, C. Meneveau, and G. L. Eyink, "Vorticity cascade and turbulent drag in wall-bounded flows: Plane Poiseuille flow," J. Fluid Mech. **974**, A27 (2023).
[16]G. P. Bewley, M. S. Paoletti, K. R. Sreenivasan, and D. P. Lathrop, "Characterization of reconnecting vortices in superfluid helium," Proc. Natl. Acad. Sci. U. S. A. **105**, 13707–13710 (2008).
[17]E. Fonda, K. R. Sreenivasan, and D. P. Lathrop, "Sub-micron solid air tracers for quantum vortices and liquid helium flows," Rev. Sci. Instrum. **87**, 025106 (2016).
[18]E. Fonda, K. R. Sreenivasan, and D. P. Lathrop, "Reconnection scaling in quantum fluids," Proc. Natl. Acad. Sci. U. S. A. **116**, 1924–1928 (2019).
[19]R. P. Feynman, "Application of quantum mechanics to liquid helium," in *Progress in Low Temperature Physics*, Vol. 1, edited by C. Gorter (North-Holland, Amsterdam, 1955), pp. 17–51.
[20]K. R. Sreenivasan, "A unified view of the origin and morphology of the turbulent boundary layer structure," in *Turbulence Management and Relaminarisation: Proceedings of the IUTAM Symposium, Bangalore, India, 1987*, IUTAM Symposia, edited by H. Liepmann and R. Narashima (Springer, Berlin, Heidelberg, 1987), pp. 37–61.
[21]K. R. Sreenivasan and A. Sahay, "The persistence of viscous effects in the overlap region, and the mean velocity in turbulent pipe and channel flows," in *Self-Sustaining Mechanisms of Wall Turbulence*, Advances in Fluid Mechanics Vol. 15, edited by R. Panton (Computational Mechanics Pub., 1997), pp. 253–272.
[22]X. Chen and K. R. Sreenivasan, "Reynolds number scaling of the peak turbulence intensity in wall flows," J. Fluid Mech. **908**, R3 (2021).
[23]X. Chen and K. R. Sreenivasan, "Law of bounded dissipation and its consequences in turbulent wall flows," J. Fluid Mech. **933**, A20 (2022).
[24]K. R. Sreenivasan and C. M. White, "The onset of drag reduction by dilute polymer additives, and the maximum drag reduction asymptote," J. Fluid Mech. **409**, 149–164 (2000).
[25]K. R. Sreenivasan, "On the scaling of the turbulence energy dissipation rate," Phys. Fluids **27**, 1048–1051 (1984).
[26]K. R. Sreenivasan, "An update on the energy dissipation rate in isotropic turbulence," Phys. Fluids **10**, 528–529 (1998).
[27]C. Meneveau and K. Sreenivasan, "The multifractal nature of turbulent energy dissipation," J. Fluid Mech. **224**, 429–484 (1991).
[28]E. R. Huggins, "Dynamical theory and probability interpretation of the vorticity field," Phys. Rev. Lett. **26**, 1291 (1971).
[29]L. Kelvin, "On vis-viva of a liquid in motion, Cambridge and Dublin Math. J. (1849)," in *Mathematical and Physical Papers: Collected from Different Scientific Periodicals from May, 1841, to the Present Time* (C. J. Clay & Sons, Cambridge University Press, 1882), Vol. I.
[30]H. Lamb, *Hydrodynamics* (University Press, 1924).
[31]G. K. Batchelor, *An Introduction to Fluid Dynamics* (Cambridge University Press, 2000).
[32]J.-Z. Wu, H.-Y. Ma, and M.-D. Zhou, *Vorticity and Vortex Dynamics* (Springer Science & Business Media, 2007).
[33]J. l R. d'Alembert, "Theoria resistentiae quam patitur corpus in fluido motum, ex principiis omnino novis et simplissimis deducta, habita ratione tum velocitatis, figurae, et massae corporis moti, tum densitatis compressionis partium fluidi," Manuscript at Berlin-Brandenburgische Akademie der Wissenschaften, Akademie-Archiv Call No.: I-M478, 1749.
[34]J. l R. d'Alembert, "Paradoxe proposé aux géomètres sur la résistance des fluides," in *Opuscules Mathématiques* (Paris), Memoir XXXIV, Section I (Imprimerie de Chardon, 1768), Vol. 5, pp. 132–138.
[35]M. J. Lighthill, "*An informal introduction to theoretical fluid mechanics*," *IMA Monograph Series* (Clarendon Press, 1986), Vol. 2.
[36]J. C. Wu, "Theory for aerodynamic force and moment in viscous flows," AIAA J. **19**, 432–441 (1981).
[37]J. Lighthill, "Fundamentals concerning wave loading on offshore structures," J. Fluid Mech. **173**, 667–681 (1986).

[38]H. Quan and G. L. Eyink, "Onsager theory of turbulence, the Josephson-Anderson relation, and the D'Alembert paradox," arXiv:2206.05326 (2024).
[39]L. Onsager, "Statistical hydrodynamics," Nuovo Cimento **6**, 279–287 (1949).
[40]G. L. Eyink and K. R. Sreenivasan, "Onsager and the theory of hydrodynamic turbulence," Rev. Mod. Phys. **78**, 87 (2006).
[41]G. Eyink, "Onsager's 'ideal turbulence' theory," J. Fluid Mech. **988**, P1 (2024).
[42]Y. Li, E. Perlman, M. Wan, Y. Yang, C. Meneveau, R. Burns, S. Chen, A. Szalay, and G. L. Eyink, "A public turbulence database cluster and applications to study Lagrangian evolution of velocity increments in turbulence," J. Turbul. **9**, N31 (2008).
[43]J. Graham, K. Kanov, X. I. A. Yang, M. Lee, N. Malaya, C. C. Lalescu, R. Burns, G. Eyink, A. Szalay, R. D. Moser, and C. Meneveau, "A web services accessible database of turbulent channel flow and its use for testing a new integral wall model for les," J. Turbul. **17**, 181–215 (2016).
[44]The reflection symmetry of the domain is unnecessary to derive our new JA-relation, if the flow is forced by prescribing constant values of h_{in} on S_{in} and h_{out} on S_{out}, and these surfaces in that case may even be curved. This driving corresponds to solving the Poisson equation for pressure p with mixed Dirichlet–Neumann conditions of the form $p = h_{in} - (\frac{1}{2}|\mathbf{u}|^2 + Q)$ on $S_{in}, p = h_{out} - (\frac{1}{2}|\mathbf{u}|^2 + Q)$ on S_{out}, and $\partial p/\partial n = \nu \mathbf{n} \cdot \Delta \mathbf{u}$ on S_w. With the same boundary conditions for the new reference potential ϕ_M as in (30), it is then easy to check that our proof of the Kelvin theorem and the JA-relation go through unchanged. However, in this alternative construction, there is no guarantee that $\mathbf{u}_\phi$ is C^∞ at $S_{in} = S_{out}$.
[45]L. Evans, *Partial Differential Equations*, Graduate Studies in Mathematics Vol. 19 (American Mathematical Society, 2010).
[46]See www.tfd.chalmers.se/~hani/kurser/OS_CFD_2011/OlofPenttinen/oldFiles/projectReport.pdf for O. Penttinen and H. Nilsson, "A pimpleFoam tutorial for channel flow, with respect to different LES models" (2011).
[47]H. G. Weller, G. Tabor, H. Jasak, and C. Fureby, "A tensorial approach to computational continuum mechanics using object-oriented techniques," Comput. Phys. **12**, 620–631 (1998).
[48]L. M. Trefethen and R. L. Panton, "Some unanswered questions in fluid mechanics," Appl. Mech. Rev. **43** 153–170 (1990), see F. A. Lyman, "Vorticity production at a solid boundary," p. 157.
[49]R. Panton, *Incompressible Flow* (John Wiley & Sons, 1984).
[50]B. R. Morton, "The generation and decay of vorticity," Geophys. Astrophys. Fluid Dyn. **28**, 277–308 (1984).
[51]A quick way to check this is to observe that the corresponding wall-normal component of the Lamb vector $(\mathbf{u} \times \boldsymbol{\omega})_y$, points upward, and it thus aligns with $u_{\phi y} > 0$ upstream of the bump but anti-aligns with $u_{\phi y} < 0$ downstream.
[52]Y. Du and T. Zaki, "Vorticity dynamics and Josephson-Anderson relation for flow over spheroid," *Bulletin of the American Physical Society. 76th Annual Meeting of the Division of Fluid Dynamics*, Washington, DC. Session L39: Vortex Dynamics and Vortex Flows: General (2023).
[53]D. Kivotides, J. Vassilicos, D. Samuels, and C. Barenghi, "Kelvin waves cascade in superfluid turbulence," Phys. Rev. Lett. **86**, 3080 (2001).
[54]E. Kozik and B. Svistunov, "Kelvin-wave cascade and decay of superfluid turbulence," Phys. Rev. Lett. **92**, 035301 (2004).
[55]P. Constantin and G. Iyer, "A stochastic-Lagrangian approach to the Navier–Stokes equations in domains with boundary," Ann. Appl. Probab. **21**, 1466–1492 (2011).
[56]G. L. Eyink, A. Gupta, and T. A. Zaki, "Stochastic Lagrangian dynamics of vorticity. Part 1. General theory for viscous, incompressible fluids," J. Fluid Mech. **901**, A2 (2020).
[57]G. L. Eyink, A. Gupta, and T. A. Zaki, "Stochastic Lagrangian dynamics of vorticity. Part 2. Application to near-wall channel-flow turbulence," J. Fluid Mech. **901**, A3 (2020).
[58]J. Nikuradse, "'Strömungsgesetze in rauhen rohren,' VDI-Forschungsheft 361. Beilage zu 'forschung auf dem gebiete des ingenieurwesens' ausgabe B, band 4. Translated as 'laws of flow in rough pipes,' " National Advisory Committee for Aeronautics, Technical Memorandum 1292, Washington, DC, 1950 (1933).
[59]O. Cadot, Y. Couder, A. Daerr, S. Douady, and A. Tsinober, "Energy injection in closed turbulent flows: Stirring through boundary layers versus inertial stirring," Phys. Rev. E **56**, 427 (1997).
[60]G. Gioia and P. Chakraborty, "Turbulent friction in rough pipes and the energy spectrum of the phenomenological theory," Phys. Rev. Lett. **96**, 044502 (2006).
[61]N. Goldenfeld, "Roughness-induced critical phenomena in a turbulent flow," Phys. Rev. Lett. **96**, 044503 (2006).
[62]J. Gao, K. Agarwal, and J. Katz, "Experimental investigation of the three-dimensional flow structure around a pair of cubes immersed in the inner part of a turbulent channel flow," J. Fluid Mech. **918**, A31 (2021).
[63]H. Quan and G. L. Eyink, "Inertial momentum dissipation for viscosity solutions of Euler equations. I. Flow around a smooth body," arXiv:2206.05325 (2022).
[64]S. Kumar, S. Toedtli, T. A. Zaki, and G. L. Eyink, "Josephson-Anderson relation as diagnostic of turbulent drag reduction by polymers" (submitted) (2024).
[65]M. Aghaei-Jouybari, J.-H. Seo, J. Yuan, R. Mittal, and C. Meneveau, "Contributions to pressure drag in rough-wall turbulent flows: Insights from force partitioning," Phys. Rev. Fluids **7**, 084602 (2022).
[66]K. Menon and R. Mittal, "On the initiation and sustenance of flow-induced vibration of cylinders: Insights from force partitioning," J. Fluid Mech. **907**, A37 (2021).
[67]K. Menon and R. Mittal, "Significance of the strain-dominated region around a vortex on induced aerodynamic loads," J. Fluid Mech. **918**, R3 (2021).
[68]K. Fukagata, K. Iwamoto, and N. Kasagi, "Contribution of Reynolds stress distribution to the skin friction in wall-bounded flows," Phys. Fluids **14**, L73–L76 (2002).
[69]M. Yoon, J. Ahn, J. Hwang, and H. J. Sung, "Contribution of velocity-vorticity correlations to the frictional drag in wall-bounded turbulent flows," Phys. Fluids **28**, 081702 (2016).